nature electronics

Supplementary information

https://doi.org/10.1038/s41928-024-01293-y

An n-doped capacitive transparent conductor for all-polymer electrochromic displays

In the format provided by the authors and unedited

Supplementary Notes

1. Comparison of conductivity and transmittance of *n*-PBDF and characterization using AFM and FTIR ---------- S3
2. Comparison of color changing properties of *n*-PBDF and PEDOT:PSS ---------- S4
3. Comparison of capacitance and transmittance of *n*-PBDF and ITO ---------- S5
4. Impact of deep LUMO level on optical and electrochemical property of *n*-PBDF --------- S6
5. Patterning of all-polymer components for electrochromic display ---------- S7
6. Uniformity of *n*-PBDF films in large-area ---------- S8

Supplementary Figures

1. Figure of metits comparison in capacitive transparent conductors ---------- S9
2. AFM results of *n*-PBDF films with different thikcness ---------- S9
3. FTIR results of *n*-PBDF films ---------- S9
4. CV and absorption properties of *n*-PBDF films ---------- S10
5. Absorption properties of PEDOT:PSS films ---------- S10
6. CV results of *n*-PBDF and *p*-type electrochromic polymers ---------- S10
7. Chemical structures of electrochromic polymers ---------- S11
8. CV results and absorption properties of *n*-PBDF, ITO, and ITO nanoparticle films ------ S11
9. Absorbance and recored current of *n*-PBDF and PEDOT:PSS films in different CV switching ---------- S12
10. Differential anodic/cathodic current density of *n*-PBDF films ---------- S12
11. Specific volumetric capacitance of *n*-PBDF films ---------- S13
12. Calculated *b* values of *n*-PBDF films ---------- S13
13. CV results of *n*-PBDF films with and without redox reaction ---------- S13
14. Photographic images of ECP-B ECDs ---------- S14
15. Absorption properties of ECP-B ECDs with ITO working electrode and VO_x ---------- S14
16. Transmittance change in ECP-B ECDs in open circuit potential condition ---------- S14
17. Optical memory of different electrochromic polymers with *n*-PBDF ---------- S15
18. Optical memory of ECP-B ECDs with *n*-PBDF ---------- S15
19. Transmittance change of ECP-B ECDs with *n*-PBDF ---------- S15
20. Transmittance change of ECP-B ECDs in continuous switching for 11 h ---------- S16
21. Transmittance change of ECP-B ECDs in environmetal stability test ---------- S16
22. Optical microscopic images of patterned electrochromic polymers ---------- S17
23. Optical photographic images of patterned solid electrolyte ---------- S17
24. Optical microscopic images and depth profile of patterned solid electrolyte ---------- S18
25. Optical microscopic images of patterned *n*-PBDF films ---------- S18
26. Photographic and microscopic images of *n*-PBDF films at large-area ---------- S19

27. Conductivity mapping of *n*-PBDF films at large-area ---------- S19
28. Ionic conductivity of solid electrolyte at 25 ℃ ---------- S19
29. Absorption spectra of ECP-B ECDs with different solid electrolyte ---------- S20
30. Transmittance change of ECP-B ECDs with different solid electrolyte ---------- S20
31. Coloration and bleaching time of ECP-B ECDs with different solid electrolyte --------- S21
32. Schematic diagram of fabrication process of counter electrodes ---------- S21
33. Optical microscopic images of patterned solid electrolyte for counter electrode -------- S22
34. Photographic images of crosstalk in passive-matrix displays ---------- S22
35. Photographic images for two-pixel representation in passive-matrix displays ---------- S22
36. Photographic images of passive-matrix displays in different pixel bleaching ---------- S23
37. Photographic images of passive-matrix displays at –0.8 V ---------- S23
38. Current of passive-matrix display for energy consumption estimation ---------- S23
39. Absorbance properties of passive-matrix displays at different applied voltages --------- S24
40. Photographic images of passive-matrix displays at different applied voltages ---------- S24
41. Normalized absorbance properties of passive-matrix displays ---------- S25
42. Measured applied voltages of passive-matrix displays ---------- S25
43. Microscopic images of patterned ECP-B and ECP-M ---------- S26
44. Phogographic images of ECDs with patterend ECP-B and ECP-M ---------- S26
45. Optical microscopic images of full-color electrochromic displays ---------- S27
46. Current of electrochromic displays in different bending radius ---------- S28
47. Photographic images of flexible electrochromic displays ---------- S28
48. Microscopic images of *n*-PBDF films on PET substrates ---------- S29
49. Photographic images of all-polymer segmented electrochromic displays ---------- S29
50. Photographic images all-polymer segmented displays on human finger ---------- S29

Supplementary Tables

1. Figure of merits of various capacitive transparent conductors ---------- S30
2. Oxidation potential and energy levels of five electrochromic polymers ---------- S30

Supplementary Videos

1. Passive-matrix electrochromic display with 8 × 8 matrix ---------- S31
2. All-polymer electrochromic display with 64 colors ---------- S31
3. Segmented all-polymer electrochromic display ---------- S31

References ---------- S32

Supplementary Note 1 Comparison of conductivity and transmittance of *n*-PBDF and characterization using AFM and FTIR

The figure-of-merits of *n*-PBDF as a capacitive transparent conductors were compared with those of other capacitive transparent conductors, such as ITO, ITO nanoparticles (used in transparent capacitor), and PEDOT:PSS as shown in **Supplementary Table 1**. The polymer films were fabricated using solution spin coating, followed only thermal annealing or drying to remove residual solvent, without any additional chemical treatment. Different thickness of *n*-PBDF films were fabricated to optimize the conductivity and optical transmittance (**Supplementary Fig. 1a**). They exhibited similar conductivity independent of the film thickness, except for 8 nm-thick film which showed a relatively reduced average conductivity of 860 S cm^{-1}. Other thicker films showed around 2000 S cm^{-1}, which is better than that of as-cast PEDOT:PSS films and comparable to that of commercial ITO in the same order (**Supplementary Fig. 1b**). The lowest conductivity was observed in ITO nanoparticle films, which are often used in high-performance transparent capacitors.

Morphological changes of *n*-PBDF at the microscale were studied depending on the film thickness using atomic force microscopy (AFM) as shown in **Supplementary Fig. 2**. All *n*-PBDF films thicker than 8 nm showed fully covered, smooth morphologies which have small nanoaggregates. In contrast, 8 nm-thick film showed partially covered aggregates. The rugged films may contribute the poor electrical conductivity. Fourier transform infrared (FTIR) spectroscopy results revealed polymer characteristics in the thin film (**Supplementary Fig. 3**). A strong bands at 1780 cm^{-1} and 1630 cm^{-1} can be assigned to the C=O stretch and C=C stretch in the aromatic ring of polymer[S1].

Supplementary Note 2 Comparison of color changing properties of *n*-PBDF and PEDOT:PSS

Indeed, *n*-PBDF conductors exhibited minimal color changes during the full-range electrochemical reaction as compared to outstanding *p*-type conductor, PEDOT:PSS (**Fig. 1e** and **Supplementary Fig. 5**). For comparison, PEDOT:PSS films were fabricated without other additional post treatment which functionalize PEDOT:PSS more. In identical thickness of polymer films (~ 30 nm), two polymeric conductors exhibited similar brightness changes from 98 to 92. However, the PEDOT:PSS showed significant color changes, with a pronounced blue and moderate greenish shift at –1.0 V bias. Quantitatively, PEDOT:PSS exhibited much severe changes in chroma ($\Delta C^* = \sqrt{\Delta a^{*2} + \Delta b^{*2}} \sim 7.13$) and total color difference ($\Delta E^* = \sqrt{\Delta L^{*2} + \Delta a^{*2} + \Delta b^{*2}} \sim 10.8$) compared to *n*-PBDF ($\Delta C^* \sim 0.78$ and $\Delta E^* \sim 5.9$, respectively). These changes are detrimental to its use as a transparent conductor, especially when employed as a counter electrode in ECDs. When the conventional *p*-type ECP at the working electrode is bleached at a positive voltage, it results in strong reduction of the counter materials and color changes. In addition, the coloration effect could occur at conductors on working electrode because of partial redox reaction of conductors by unintended charge transfer or remained voltage bias for the *p*-type ECP coloration. In contrast, *n*-PBDF displayed minimal color changes from reduced (–0.4 V) to oxidized (+1.0 V) states, regardless of film thickness, which suggests its suitability for use of transparent conductors for both working and counter electrodes.

Supplementary Note 3 Comparison of capacitance and transmittance of *n*-PBDF and ITO

To investigate capacitive behavior of *n*-PBDF in comparison with inorganic counterpart ITO, CV characteristics and transmittance change under the electrochemical reaction were measured (**Supplementary Fig. 8**). Indeed, *n*-PBDF films exhibited much higher volumetric capacitance higher than 200 F cm^{-3} compared to sputtered ITO thin film (180 nm; 0.75 F cm^{-3}) and ITO nanoparticle film (1.7 μm; 9.19 F cm^{-3}). It is because the inorganic layer relied on capacitance involving only electrical double layer on surface of film or nanoparticles. Their conductivity and capacitance were compared as shown in **Supplementary Fig. 1b**. Two polymer conductors exhibited both high conductivity and capacitance due to their mixed high ionic and electronic conductive nature. In contrast, ITO film showed low capacitance because ions cannot penetrate rigid inorganic film and cannot form large surface electrical double layer. The ion penetration could be enhanced using nanostructure engineering, but it reversely reduced electrical conductivity.

Meanwhile, the pure capacitive behavior benefits minimal color changes under electrochemical bias (**Supplementary Fig. 8b** and **c**). Other two polymer conductors exhibited relatively reduced transmittance at fully de-doped state because reversible redox reactions also contribute the high volumetric capacitance (**Supplementary Fig. 8d**). *n*-PBDF showed relatively small color and optical transmittance change in visible region because their main absorption peak occurs at 877 nm (**Fig. 1c**–**d** and **Supplementary Fig. 4c**–**d**). In addition, two polymer conductors showed the broad high doping range and large non-faradaic capacitance (**Supplementary Note 4** and **Supplementary Fig. 9**). Through ECD operation voltage modulation by considering oxidation/reduction potential of ECPs, one could control color changes and capacitance of counter ion storage layer during the electrochemical reactions.

Supplementary Note 4 Impact of deep LUMO level on optical and electrochemical property of *n*-PBDF

The other interesting property of the *n*-PBDF for electrochromic devices is deeply engineered LUMO level (~ –5.1 eV), which enabled *n*-doped conductor application in ambient condition by avoiding water and oxygen reduction reactions[S2]. First, they can give rise to stable and strong capacitive behavior from electrical double layer due to small doping changes without unwanted charge transfer to/from oxygen nor poor charge injection/transport in strongly undoped state[S3]. In addition, the easy doping or low reduction potential due to such the low LUMO level could be utilized for high-performance all-polymer electrochromic devices, allowing a broader bleached states in electroactive region. They easily retain the doped state and the resultant transparent nature until around +0.7 V bias (**Fig. 1c**). They showed a distinct increase in visible absorption at applied voltage higher than +0.8 V because of the very weak dedoping ability. Additionally, optical absorption was recorded in different CV switching range of *n*-PBDF films (**Supplementary Fig. 9**). The absorption changes were highly reduced when the electrochemical switching was limited within high doping range (–0.5 to +0.5 V). Meanwhile, they showed comparable capacitance from pure capacitance (196 F cm^{-3}) to that from both redox and pure capacitive behavior (235 F cm^{-3}). PEDOT:PSS also showed similar strong pure capacitive behavior due to their high mixed ionic and electronic conductivity.

The low onset reduction potential (~ +0.7 V) brings about a larger potential window by capacitive electrical double layer and efficient electroactive matching to that of the conventional *p*-type electrochromic polymers (**Fig. 1f**, **Supplementary Fig. 4b** and **6**). When conventional *n*-type transition metal oxides or non-conductive *n*-type polymers are used as the ion-storage material in an unbalanced configuration, the charge-balanced voltages applied to the counter electrodes is extended to the more negative end[S4]. The extremely low reduction potential in PBDF allows a closed matched electroactive voltage window with the *p*-type polymer, the voltage applied at the counter electrode is much less negative. The low reduction potential and narrow operation voltage prevents the electrochemical degradation caused by over-oxidation in both *p*-type electrochromic polymers and *n*-PBDF, leading to the better cycling stability in electrochromic devices[S4, 5].

Supplementary Note 5 Patterning of all-polymer components for electrochromic display

For high flexibility and human-friendly nature in see-through display demonstration, transparent polymer components were utilized such as electrochromic active materials, electrolytes, ion storage layers, and electrodes as depicted in **Fig. 3a**. Five colors of ECPs based on poly(3,4-propylenedioxythiophene) (PProDOT) were studied for demonstration of diverse color representation in the display application. The ECPs are denoted as ECP-C, ECP-M, ECP-Y, ECP-K, and ECP-B for cyan, magenta, yellow, black, and blue colors, respectively as shown in photographic images (**Fig. 3b**). A simple, one step photolithographic micropatterning is enabled from preparation of electrochromic polymer solution in presence of a bis(fluorophenylazide) (bisFA) crosslinker, which induces a large solvent resistances via photocrosslinking by nitrene insertion into the alkyl side chains of ECPs[S6, 7]. With good-solvent treatment (e.g., toluene, chloroform, and dichloromethane) for pattern development, high resolution micropatterns could be realized on the glass following mask-blocked near-UV light illumination (~2000 mJ cm^{-2}; 405 nm) as shown in **Fig. 3c** and **Supplementary Fig. 22**.

Patterning of an ionic conductor for solid electrolyte layer in ECDs was also realized using photopolymerization of acrylate groups in presence with ionic liquid and thiol monomer (See **Method** section for detailed fabrication methods). The thiol monomer enabled the free radical photopolymerization for both chain-growth and step-growth in polyethylene glycol diacrylate (PEGDA), leading to reduced polymerization time and the high energy efficiency in photolithography process[S8, 9]. In addition, the use of ionic liquid without additional polar solvent as well as addition of the thiol molecules enhances a wettability of the precursor solution on various surface in display application (e.g., metal oxides [VO_x], glass, ITO, and polymeric layers), which enabled fabrication of size-tunable, patterned solid electrolyte layer using simple spin coating process up to several hundreds of nanometer thickness. Upon the selective UV light illumination and removal of uncured portion, micro-sized patterns could be developed through the direct photolithography (**Fig. 3d**, **Supplementary Fig. 23** and **24**).

A newly developed *n*-type conducting polymer, *n*-PBDF was used for the transparent conductors and conducting ion-storge layer in ECDs here. In polymerization and ink preparation process, they immediately undergo reductive doping through water oxidation to yield *n*-doped PBDF, leading to very stable enhancement of electrical conductivity and low absorption coefficient in a visible region[S1]. Patterning of the *n*-PBDF thin films fabricated spin-coating process is realized by photolithography in combination with reactive ion etching (RIE) dry process and etch-blocking layer. The conducting polymer films were chemically and mechanically robust from thermal treatment and orthogonal solution processing in photolithography process, leading to clear microscale patterns with sharp edge (**Fig. 3e** and **Supplementary Fig. 25**).

Supplementary Note 6 Uniformity of *n*-PBDF films in large-area

Film uniformity of spin coated *n*-PBDF films on large-scale (5.0×7.5 cm^2) glass substrate was studied using optical microscopic images at different positions and conductivity mapping using R50-4PP mapping machine (Filmetrics). Optical microscopy results revealed smooth and clean surface in almost parts of the films (**Supplementary Fig. 26**). We easily observed certain streaks on edge of the films due to coffee ring effect during spin coating and solvent drying process. Still, the optical microscopic images show the smooth surface except the non-uniform solvent dried part. For large-area display applications, we investigate conductivity mapping of films (**Supplementary Fig. 27**). We mapped sheet resistance at total 5×15 = 75 points in 5.0×7.5 cm^2 substrate. The sheet resistances were recorded at different points with equal distance considering 0.5 cm edge exclusion using the mapping machine software. Thickness for conductivity calculations was measured using AFM at different points. Conductivity was calculated using identical method for various capacitive transparent conductors on 2.5×2.5 cm^2 glass substrate as shown in **Supplementary Note 1**. Average and standard deviation of conductivity were 1750 and ±95 S cm^{-1}, respectively. The optical microscopic images and conductivity mapping results revealed quite uniform film quality in the relatively large-scale (5.0×7.5 cm^2), spin-coated films for electrochromic display application in this work.

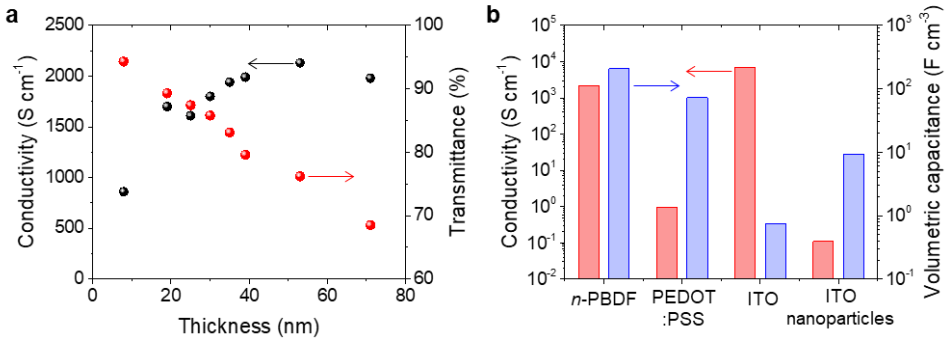

Supplementary Fig. 1. a) Conductivity and transmittance of *n*-PBDF films depending on the film thickness. **b**) Conductivity and volumetric capacitance comparison of capacitive transparent conductors.

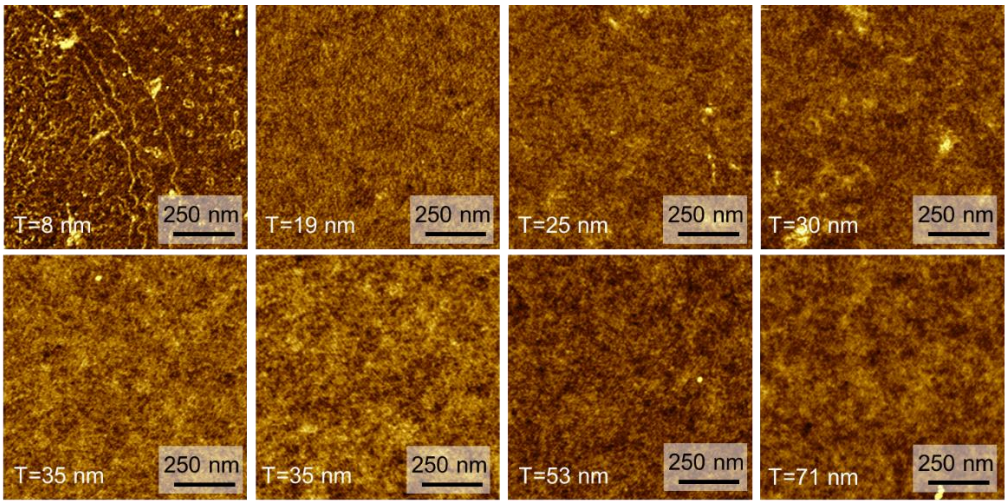

Supplementary Fig. 2. AFM measurement results of *n*-PBDF films as a function of thickness.

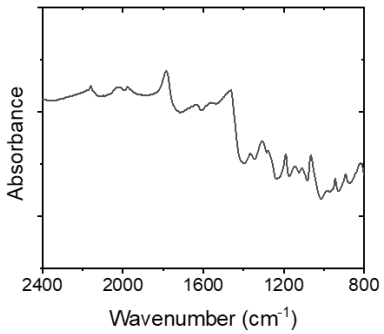

Supplementary Fig. 3. FTIR measurement results of *n*-PBDF thin films on glass substrate.

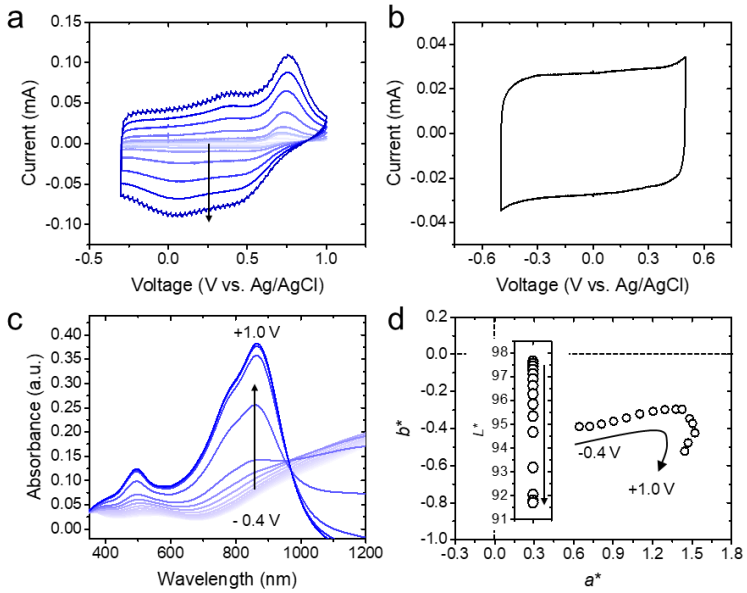

Supplementary Fig. 4. a) CV results of ECDs based on the thin *n*-PBDF films (20 nm) for conductor on working electrode. Results were recorded in different scan speed, following the arrow of 1, 3, 5, 10, 25, 50, 75 and 100 mV s^{-1}. **b**) CV results of ECDs based on the *n*-PBDF films (20 nm) in a pure capacitive behavior. **c**) Optical absorbance spectra of *n*-PBDF ion storage conductive films (30 nm) for counter electrode at different doping state. All lines have equidistant potential steps of 0.1 V. **d**) CIE *L**, *a**, *b** color coordinate values of the *n*-PBDF films (30 nm) at different doping state. Data points have equidistant potential steps of 0.1 V.

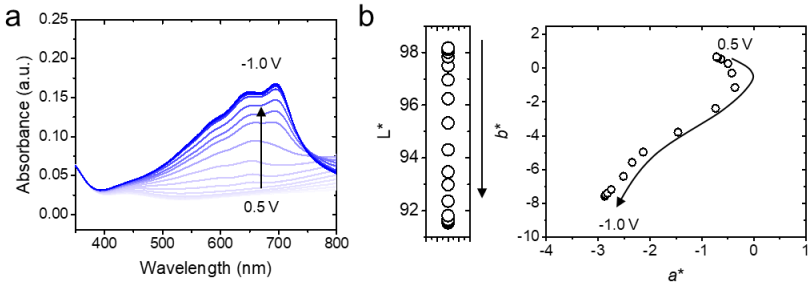

Supplementary Fig. 5. a) Optical absorbance spectra of PEDOT:PSS films (30 nm) at different doping state. All lines have equidistant potential steps of 0.1 V. **b**) CIE *L**, *a**, *b** color coordinate values of the PEDOT:PSS films (30 nm) at different doping state. Data points have equidistant potential steps of 0.1 V.

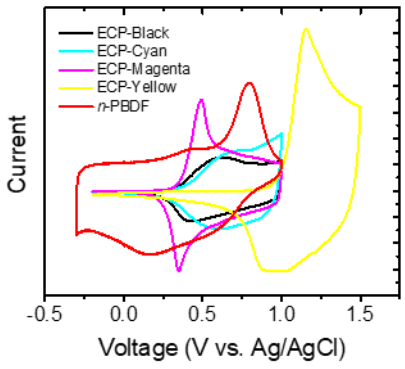

Supplementary Fig. 6. Cyclic voltammetry results of *n*-PBDF and *p*-type electrochromic polymer films.

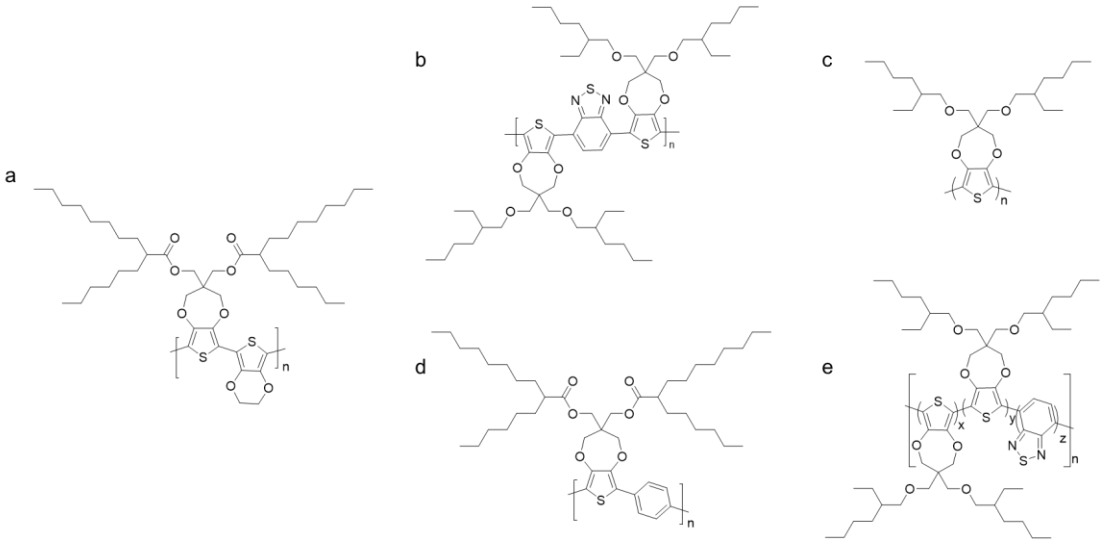

Supplementary Fig. 7. Chemical structures of blue (**a**), cyan (**b**), magenta (**c**), yellow (**d**), and black (**e**) colored *p*-type electrochromic polymers.

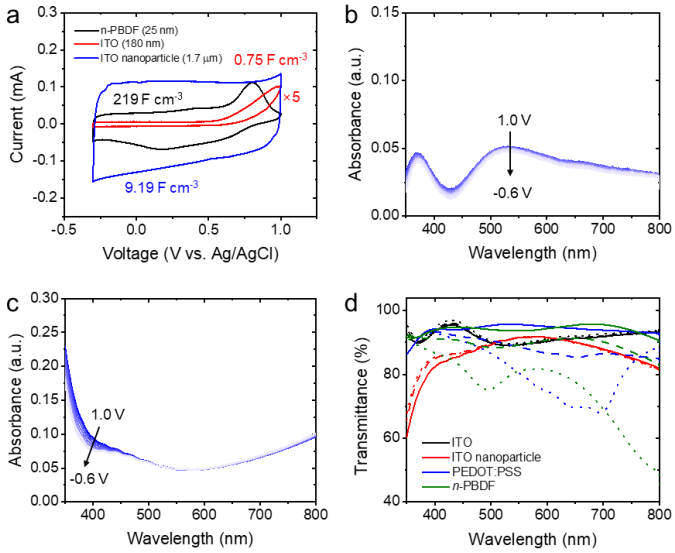

Supplementary Fig. 8. a) Cyclic voltammetry results of *n*-PBDF, ITO film, and ITO nanoparticle film. **b**–**c**) Optical absorbance spectra of ITO film (**b**) and ITO nanoparticle film (**c**) at different electrochemical voltage (vs. Ag/AgCl). All lines have equidistant potential steps of 0.2 V. **d**) Optical transmittance comparison of ITO, ITO nanoparticle films, PEDOT:PSS, and *n*-PBDF films at different electrochemical voltage (vs. Ag/AgCl). For ITO and ITO nanoparticles, solid line denotes 1.0 V, dashed one denotes 0.2 V, and dotted one denotes –0.6 V with 0.8 V steps. For PEDOT:PSS, solid line denotes 0.4 V (fully doped), dashed one denotes –0.3 V, and dotted one denotes –1.0 V (fully de-doped) with 0.7 V step. For *n*-PBDF, solid line denotes –0.4 V (fully doped), dashed one denotes 0.3 V, and dotted one denotes 1.0 V (fully de-doped) with 0.7 V step.

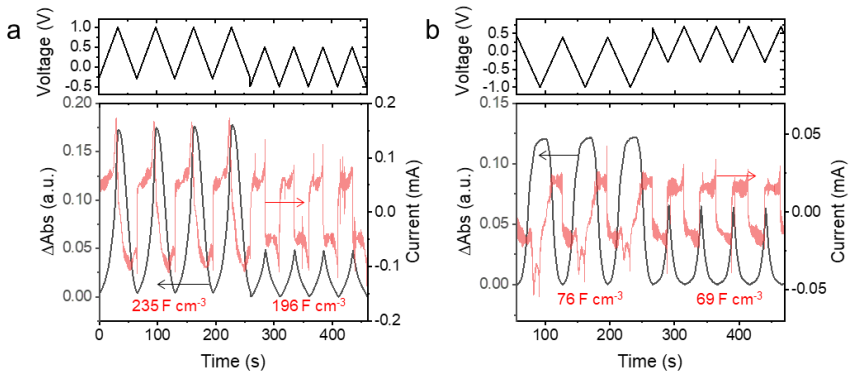

Supplementary Fig. 9. a–**b**) Optical absorbance change and recorded current of *n*-PBDF (**a**) and PEDOT:PSS (**b**) films in different CV switching. For *n*-PBDF, –0.3 V to 1.0 V and –0.5 V to 0.5 V were applied sequentially following the above voltage information. For PEDOT:PSS, –1.0 V to 0.3 V and –0.3 V to 0.7 V were applied. Volumetric specific capacitances were estimated from the CV results in two different switching ranges.

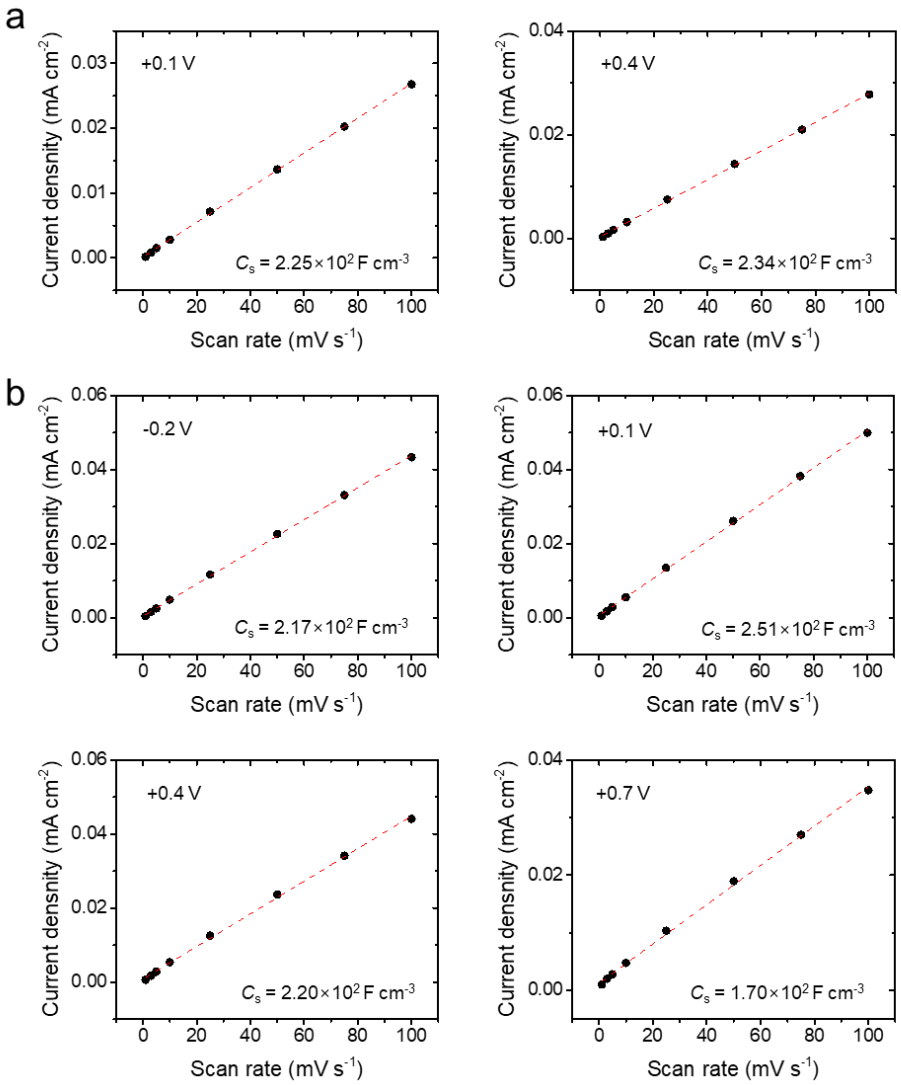

Supplementary Fig. 10. a–**b**) Differential anodic/cathodic current density of the thin (20 nm; **a**) and thick (30 nm; **b**) *n*-PBDF electrodes as function of scan rate.

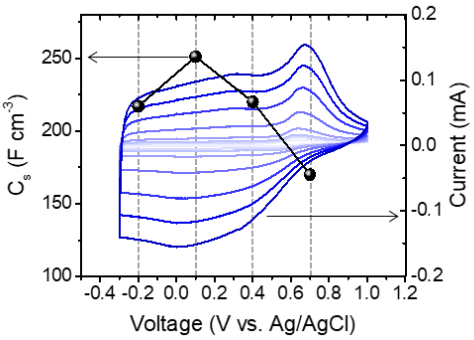

Supplementary Fig. 11. Calculated specific volumetric capacitance from differential anodic/cathodic current in different scan rate of CV at specific voltage points. Results were recorded in different scan speed; 1, 3, 5, 10, 25, 50, 75, 100 mV s^{-1}.

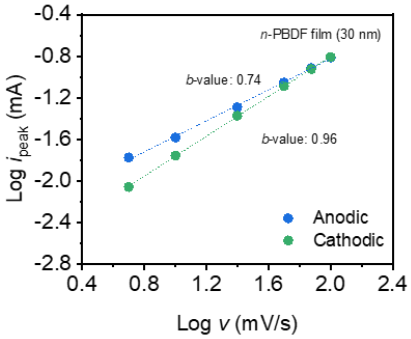

Supplementary Fig. 12. Calculated *b* values from anodic and cathodic peak currents in different scan rate of CV at specific voltage points.

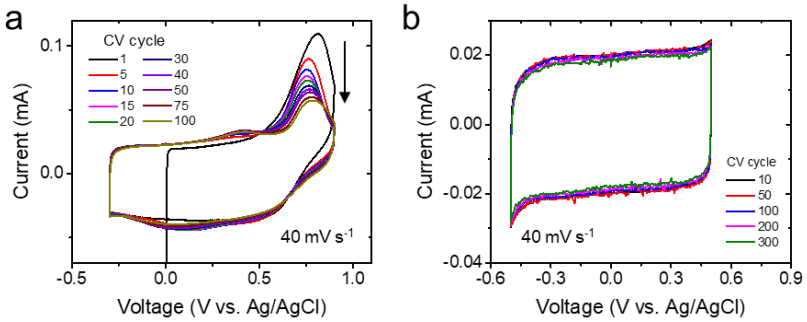

Supplementary Fig. 13. a) Cyclic voltammetry curves of *n*-PBDF films in electrochemical cycles including redox reaction. **b**) Cyclic voltammetry curves of *n*-PBDF films in electrochemical cycles without redox reaction.

Supplementary Fig. 14. Photographic images of ECP-B ECDs with *n*-PBDF electrodes for size confirmation (**a**), in colored (**b**), and bleached states (**c**).

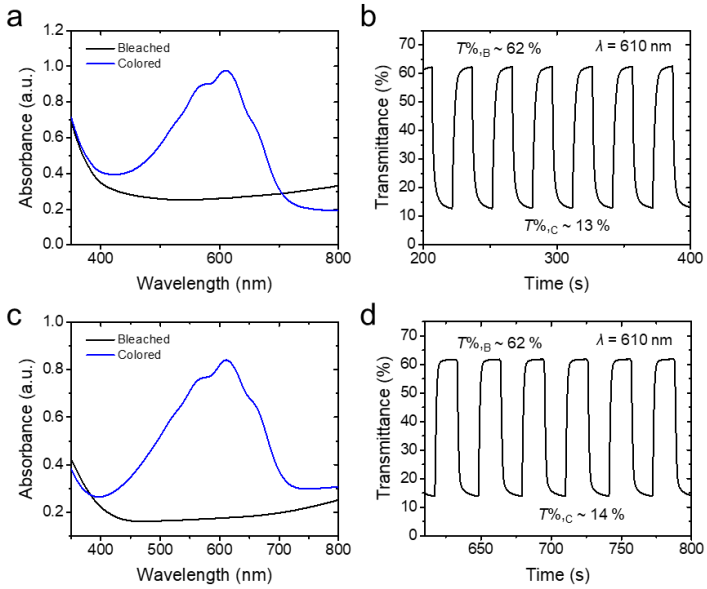

Supplementary Fig. 15. **a**) Absorption spectra of ECP-B ECDs with ITO working electrode and conventional VO_x ion storage counter electrode on ITO. **b**) Dynamic transmittance change of ECDs with ITO working electrode and conventional VO_x ion storage counter electrode on ITO. **c**) Absorption spectra of ECDs with the *n*-PBDF counter electrodes and with ITO working electrode. **d**) Dynamic transmittance change of ECDs with the *n*-PBDF counter electrodes and with ITO working electrode.

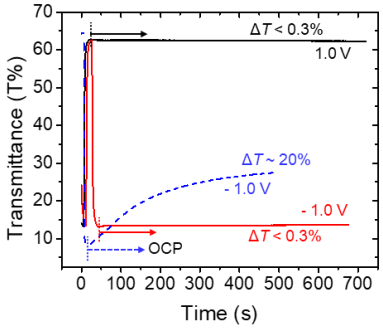

Supplementary Fig. 16. Optical transmittance change in ECP-B ECDs fabricated with conventional PC/LiTFSI-based electrolyte (dotted blue line) and the ion gel-based electrolyte (solid black and red lines) with VO_x counter electrode. The open circuit potential condition started at "OCP" region.

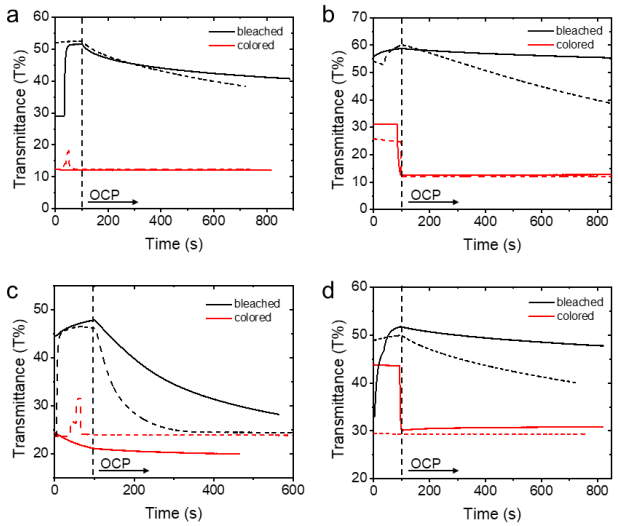

Supplementary Fig. 17. a–**d**) Optical memory of ECP-C (**a**), ECP-M (**b**), ECP-Y (**c**), and ECP-K (**d**) ECDs with the *n*-PBDF electrodes. Solid lines indicate optical memory in ionic liquid-based solid electrolyte, and dotted line indicate optical memory in PC/LiTFSI-based solid electrolyte. The open circuit potential condition started at "OCP" region.

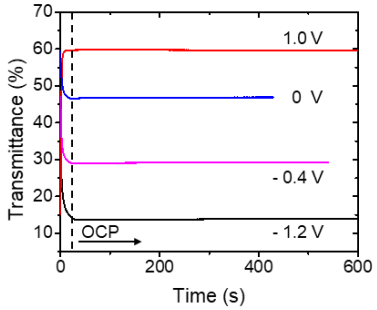

Supplementary Fig. 18. Optical memory of ECP-B ECDs with the *n*-PBDF counter electrodes and with ITO working electrode with ionic liquid-based electrolyte. The open circuit potential condition started at "OCP" region.

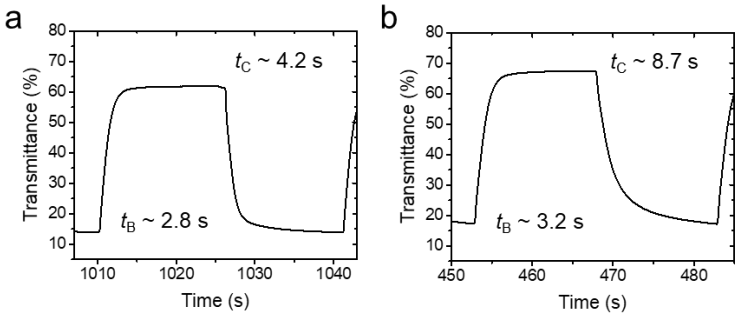

Supplementary Fig. 19. **a**, **b**) Dynamic transmittance change of ECP-B ECDs with the *n*-PBDF counter electrodes and with ITO working electrode (**a**) and based on the PBDFs as both working and counter electrodes (**b**).

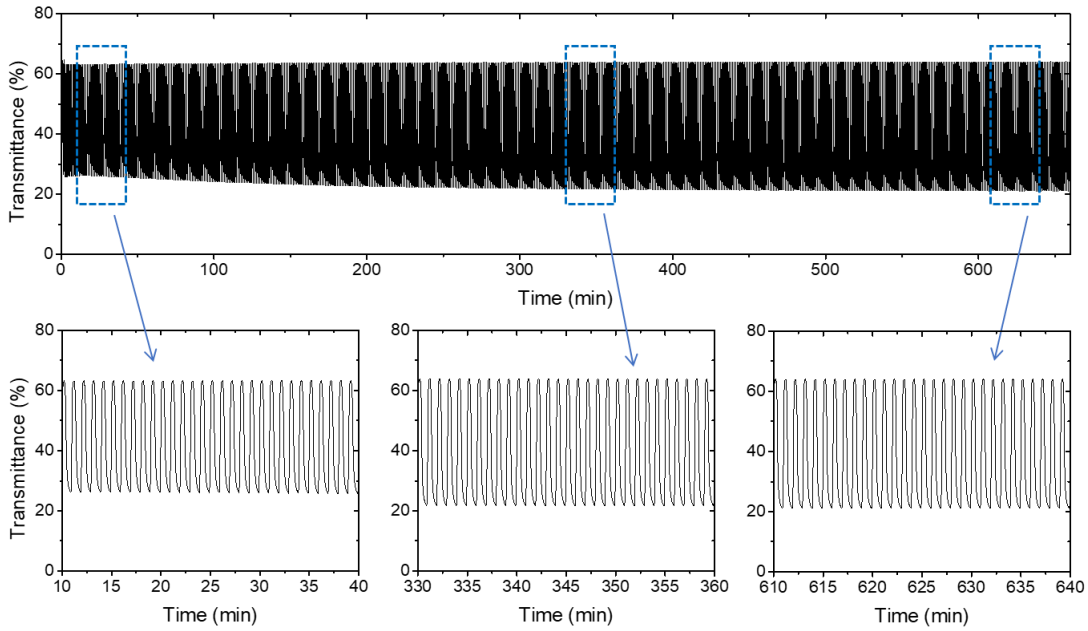

Supplementary Fig. 20. Transmittance change of ECP-B ECDs with the *n*-PBDF electrodes in continuous electrochemical switching for 11 h.

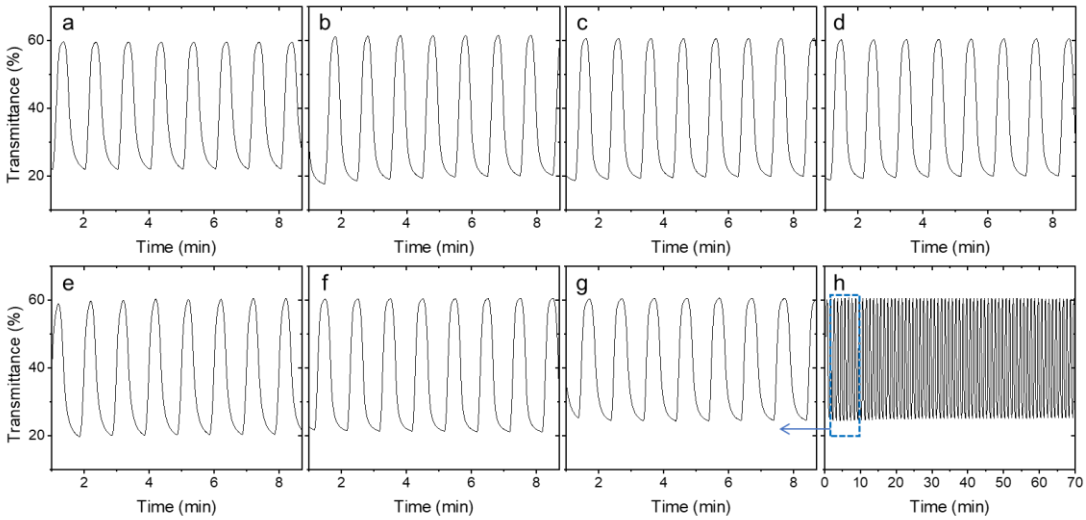

Supplementary Fig. 21. Transmittance change of ECP-B ECDs with the *n*-PBDF electrodes before environmental stability test (**a**), 30 min aged (**b**), 2 h aged (**c**), and 5 h aged (**d**) under 50 % RH/50 ℃ condition, and 1 h aged (**e**), 1day aged (**f**), and 1 week aged (**g**, **h**) under 85% RH/60 ℃ conditions. All measurements were conducted sequentially using a single ECD under the same operation voltages.

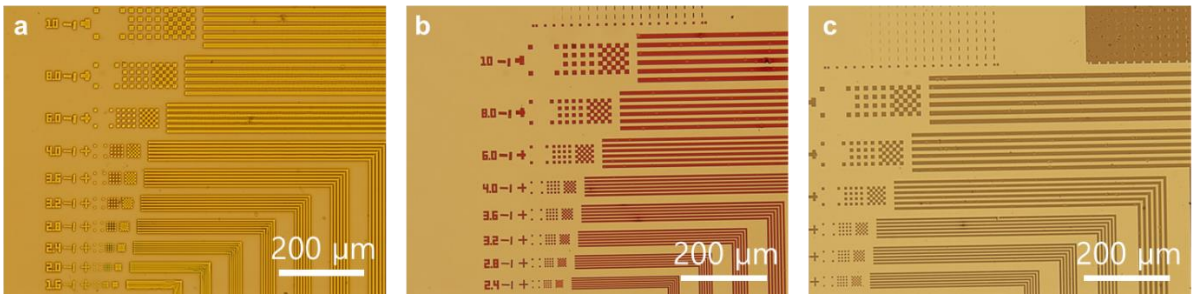

Supplementary Fig. 22. a–**c**) Optical microscopic images of patterned ECPs for yellow (**a**), magenta (**b**), and cyan (**c**) in microscale.

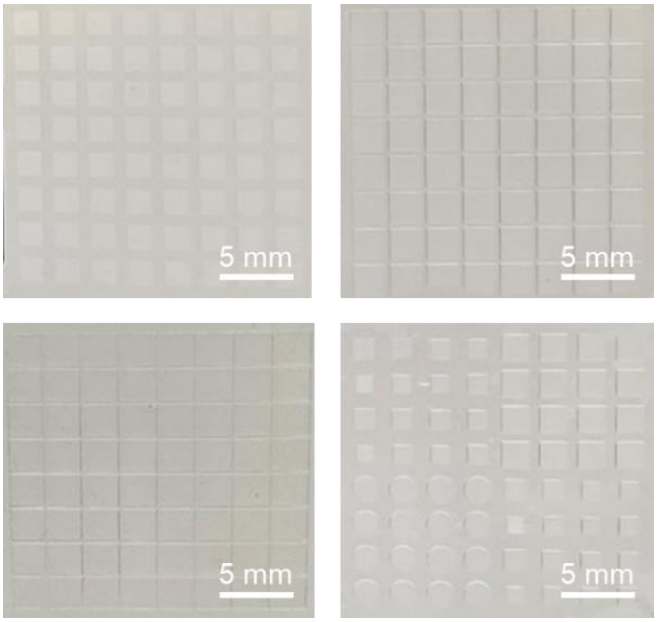

Supplementary Fig. 23. Optical photographic images of patterned solid electrolyte.

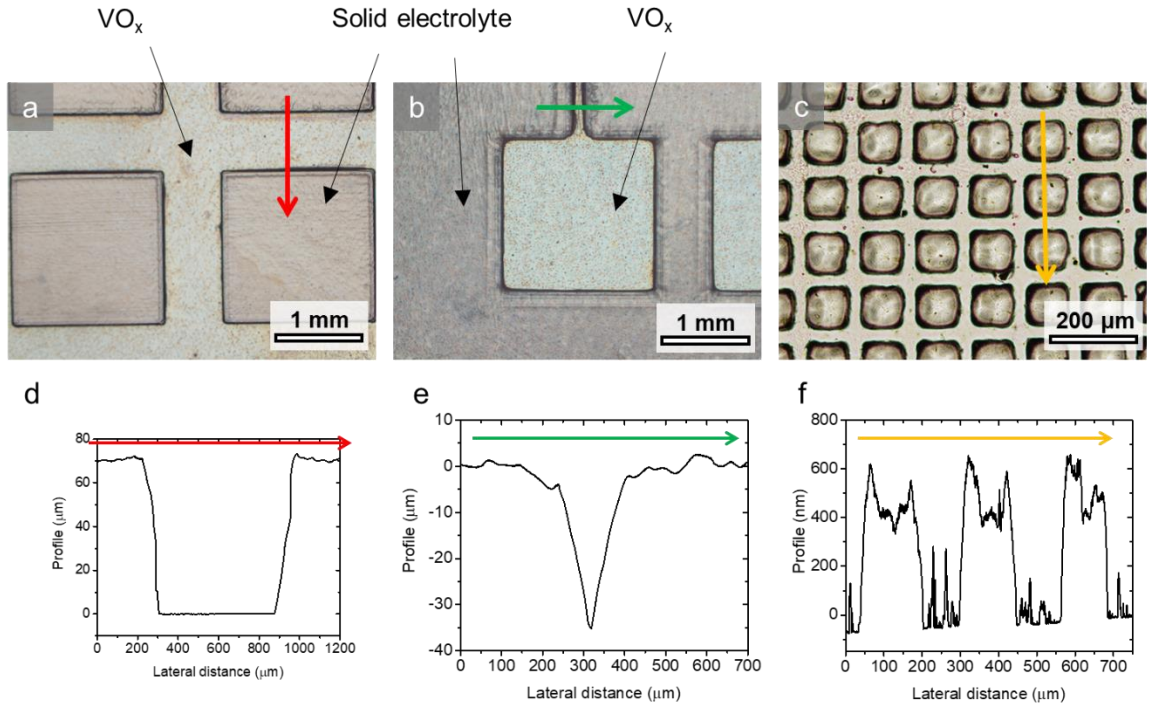

Supplementary Fig. 24. a–**c**) Optical microscopic images of patterned solid electrolyte. **d**–**f**) Depth profile results of patterned solid electrolyte.

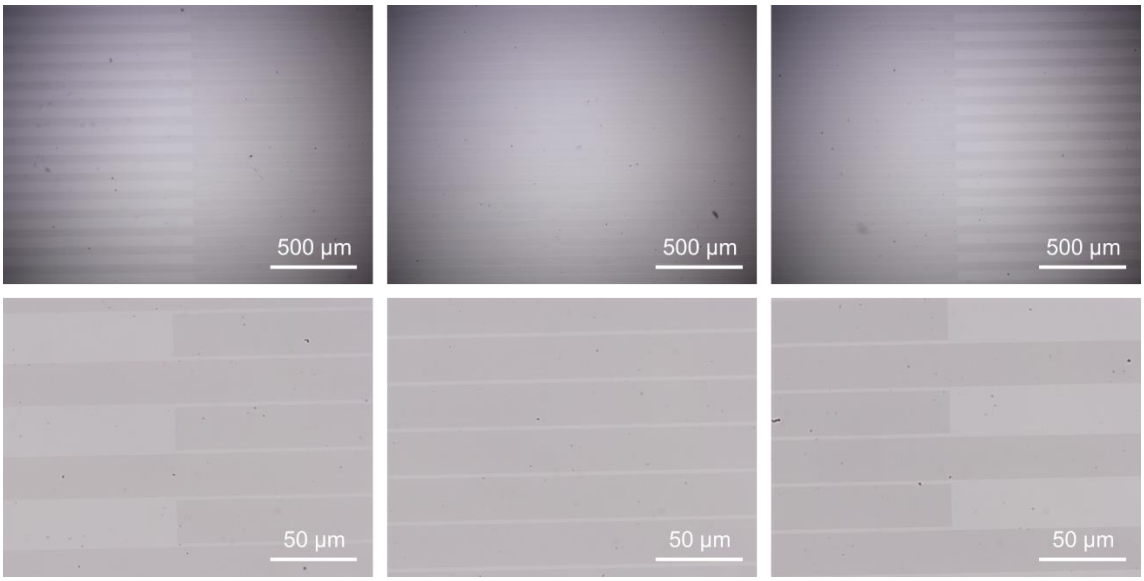

Supplementary Fig. 25. Optical microscopic images of patterned *n*-PBDFs.

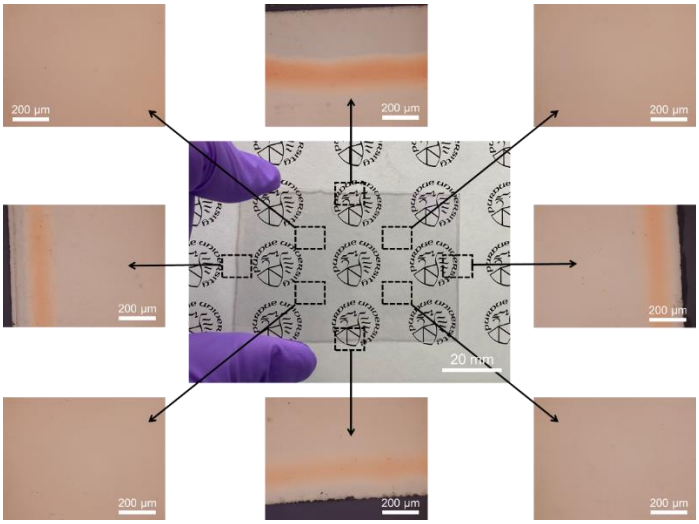

Supplementary Fig. 26. Photographic and optical microscopic images of spin-coated *n*-PBDF films on 5.0×7.5 cm^2 glass substrate for display application.

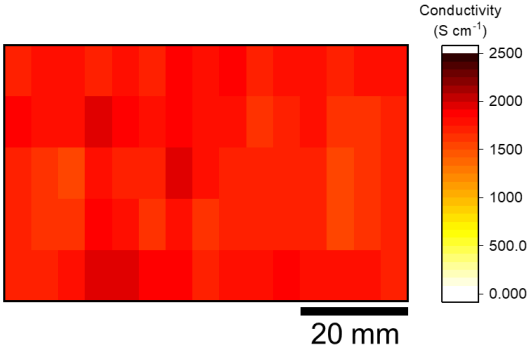

Supplementary Fig. 27. Conductivity mapping of spin-coated *n*-PBDF films on 5.0×7.5 cm^2 glass substrate for display application.

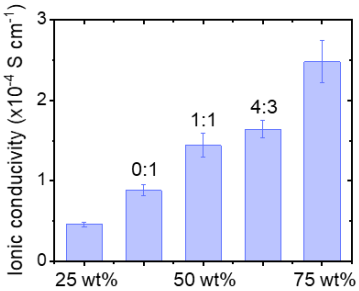

Supplementary Fig. 28. Ionic conductivity of polymeric solid electrolyte films with different blending conditions at 25 °C. The *y*-axis indicates the ionic liquid fraction, while inset values above bar charts represent blending ratio between thiol molecule and PEGDA. The average and standard deviations (error bars) values were obtained for at least six films from more than three different batches.

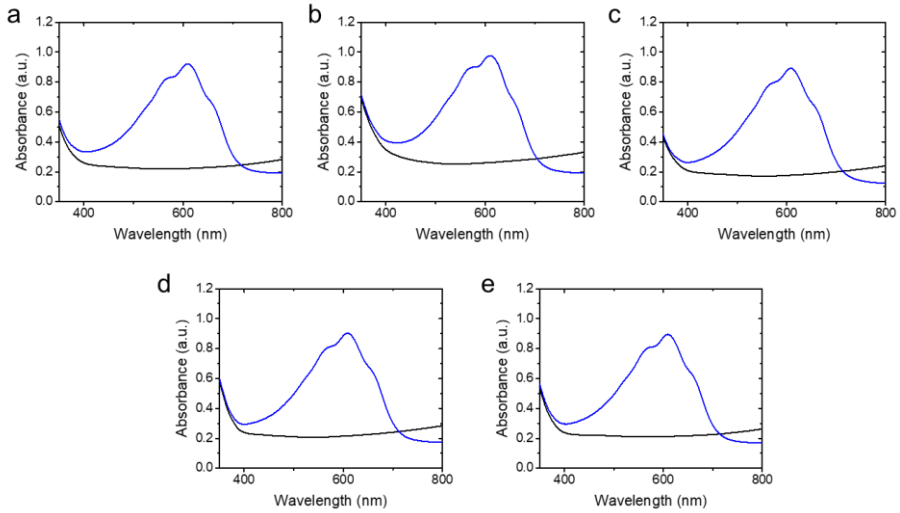

Supplementary Fig. 29. **a**–**c**) Absorption spectra of ECDs using ECP-B with the polymeric solid electrolyte with 0:1 (**a**), 1:1 (**b**), and 4:3 (**c**) of thiol monomer and PEGDA with 50wt% ionic liquid. **d**, **e**) Absorption spectra of ECDs using ECP-B with the polymeric solid electrolyte with 1:1 of thiol monomer and PEGDA with 25wt% ionic liquid (**d**) and 75wt% ionic liquid (**e**).

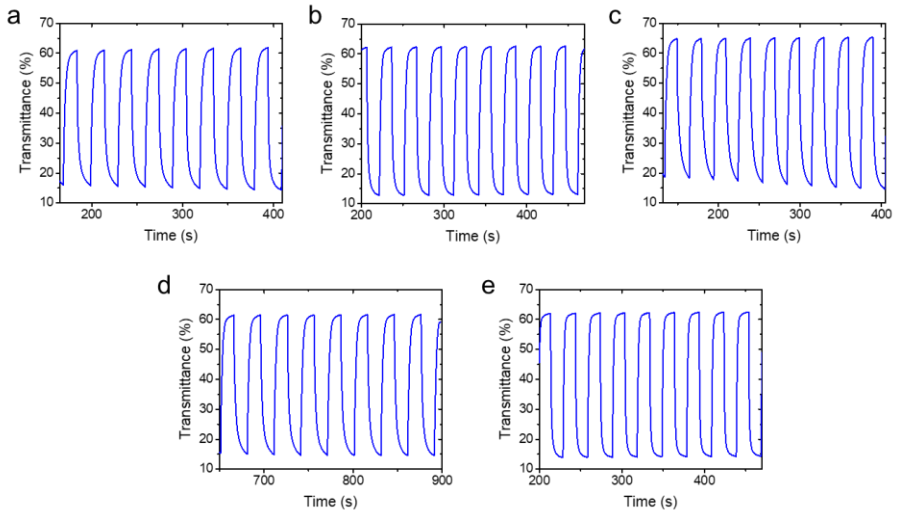

Supplementary Fig. 30. a–**c**) Dynamic transmittance of ECDs using ECP-B with the polymeric solid electrolyte with 0:1 (**a**), 1:1 (**b**), and 4:3 (**c**) of thiol monomer and PEGDA with 50wt% ionic liquid. **d**, **e**) Dynamic transmittance of ECDs using ECP-B with the polymeric solid electrolyte with 1:1 of thiol monomer and PEGDA with 25wt% ionic liquid (**d**) and 75wt% ionic liquid (**e**).

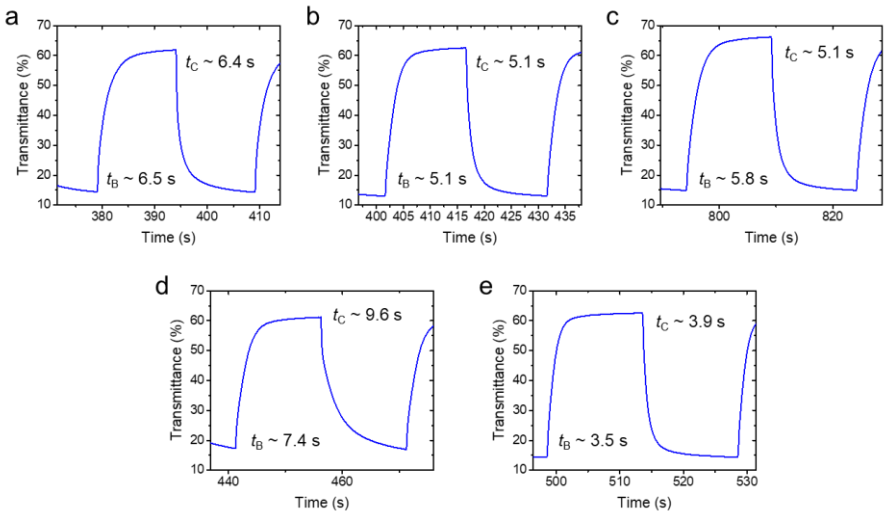

Supplementary Fig. 31. **a**–**c**) Dynamic transmittance of ECDs using ECP-B with the polymeric solid electrolyte with 0:1 (**a**), 1:1 (**b**), and 4:3 (**c**) of thiol monomer and PEGDA with 50wt% ionic liquid. **d**, **e**) Dynamic transmittance of ECDs using ECP-B with the polymeric solid electrolyte with 1:1 of thiol monomer and PEGDA with 25wt% ionic liquid (**d**) and 75wt% ionic liquid (**e**).

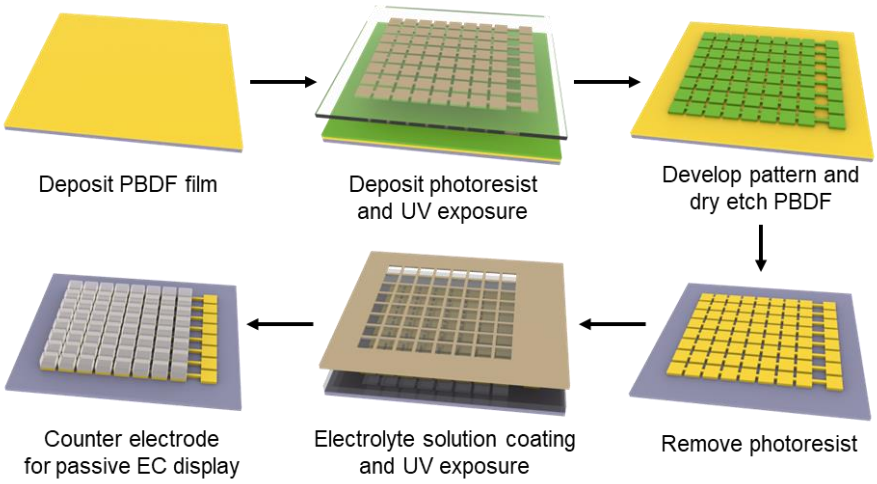

Supplementary Fig. 32. Schematic diagram of fabrication process of counter electrode part for all-polymer passive-matrix-based electrochromic display using photolithographic patterning.

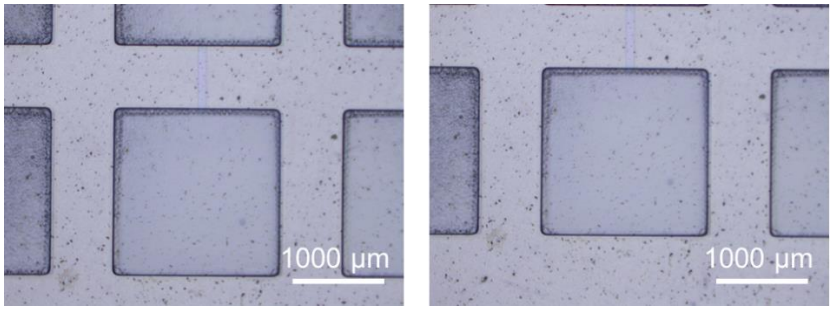

Supplementary Fig. 33. Optical microscopic images of patterned solid electrolyte for counter electrode part in passive-matrix applications.

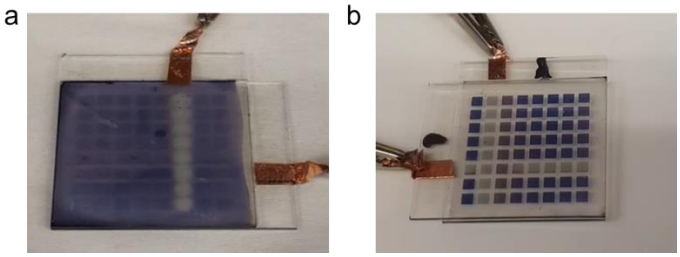

Supplementary Fig. 34. **a**, **b**) Pictures of crosstalk in non-patterned (**a**) and only polymer patterned (**b**) displays. In both displays, electrolyte was not patterned.

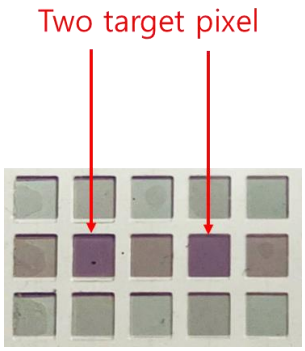

Supplementary Fig. 35. Pictures for color representation of passive-matrix-based display as two pixels were turned-on. The voltage of –0.8 V was applied for 10 s at the target pixels.

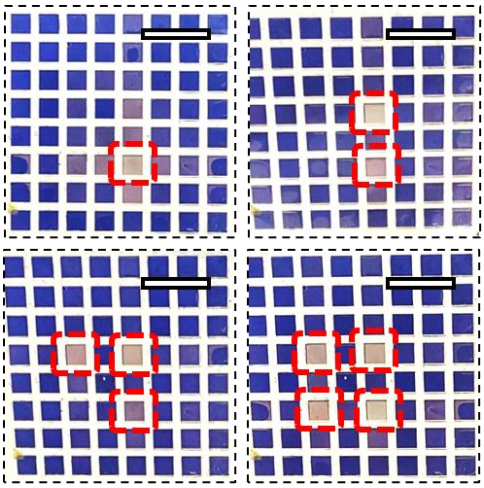

Supplementary Fig. 36. Pictures of passive-matrix displays in different pixel bleaching. Scale bar means 5 mm. The bleaching voltage (+ 1.0 V) was applied on four target pixels with 30 second intervals.

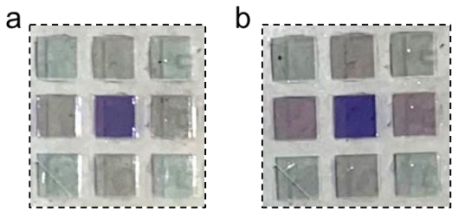

Supplementary Fig. 37. **a**, **b**) Pictures for color representation of passive-matrix-based display when the voltage of –0.8 V was applied for 10 s (**a**) and stayed at 1000 sec at open-circuit potential (**b**).

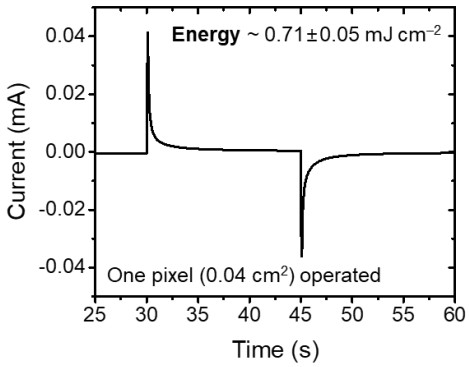

Supplementary Fig. 38. Current profile in chronoamperometry response of passive-matrix-based display when the voltage of –1.0 and +1.0 V was applied for 15 s. "**Energy**" means consumed energy one coloration/bleaching switch.

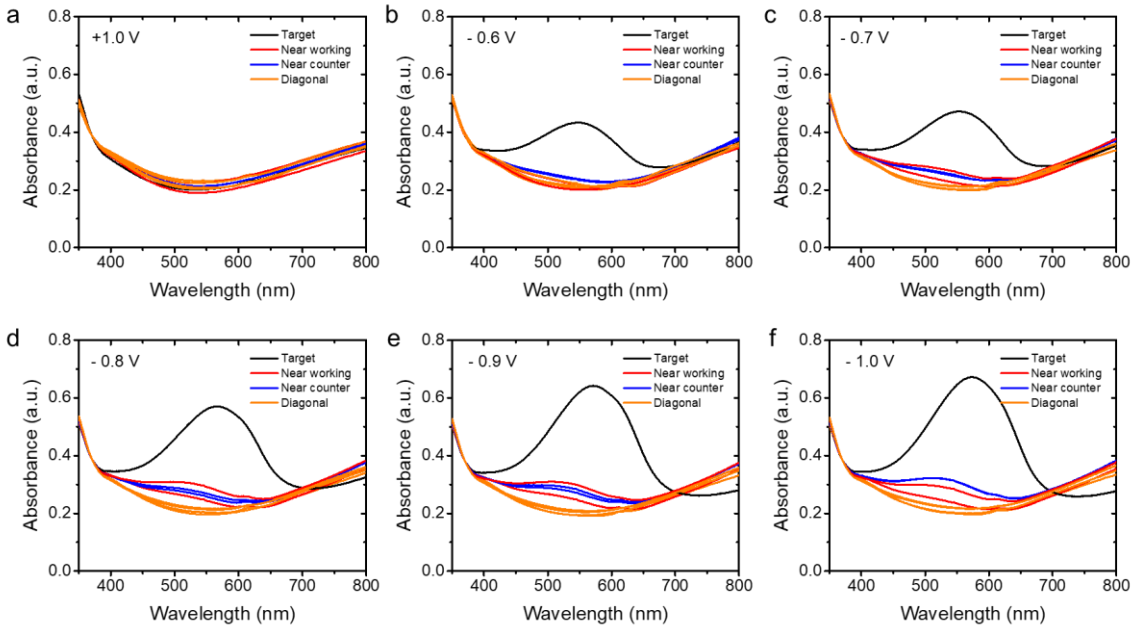

Supplementary Fig. 39. Absorbance spectra of passive-matrix-based display depending on the applied voltage at target pixel. The voltage was applied for 30 s and removed during absorbance measurement.

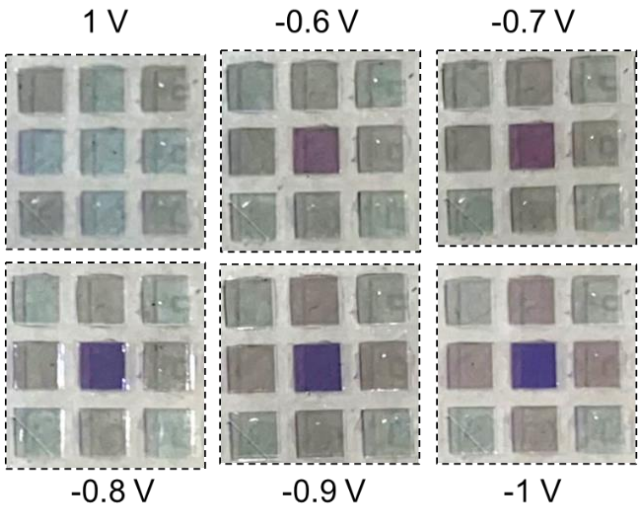

Supplementary Fig. 40. Pictures for color representation of passive-matrix-based display depending on the applied voltage at target pixel. The voltage was applied for 30 s.

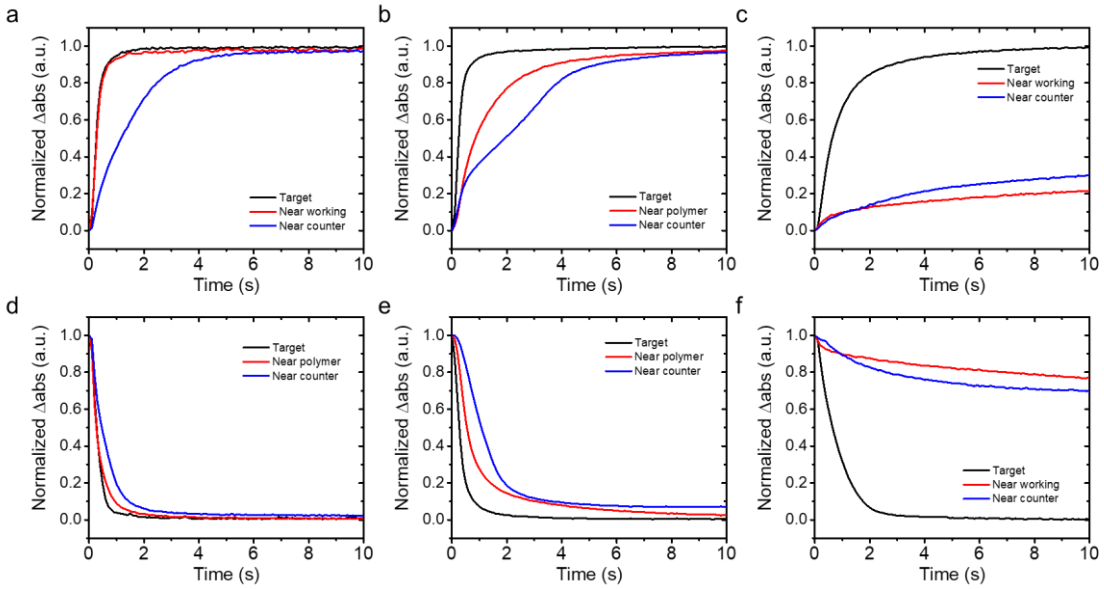

Supplementary Fig. 41. **a**–**c**) Normalized dynamic absorbance change in passive-matrix-based display in coloration process of non-patterned (**a**), only polymer patterned (**b**), and electrolyte patterned (**c**) display. **d**–**f**) Normalized dynamic absorbance change in passive-matrix-based display in bleaching process of non-patterned (**d**), only polymer patterned (**e**), and electrolyte patterned (**f**) display.

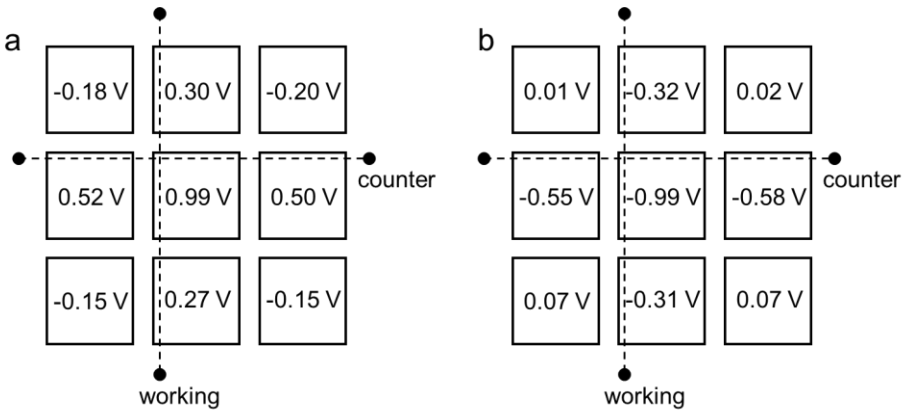

Supplementary Fig. 42. **a**, **b**) Measured applied voltages at 9 pixels when 1.0 V (**a**) and –1.0 V (**b**) was applied at only target pixel.

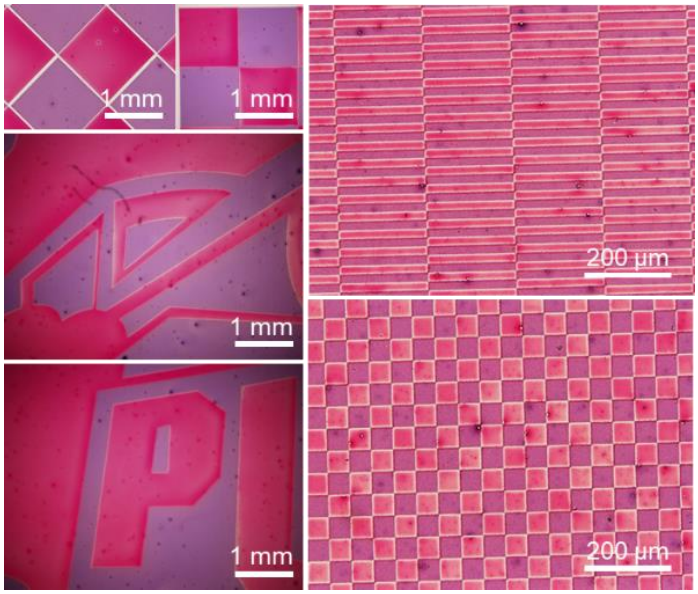

Supplementary Fig. 43. Optical microscopic images of ECDs with patterned ECP-B and M.

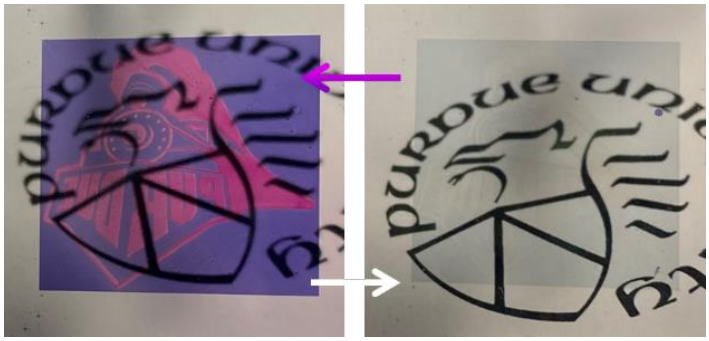

Supplementary Fig. 44. Photographic images of ECDs with patterned ECP-B and M when they are reduced (colored with –1.0 V; left) and oxidized (bleached with +1.0 V; right).

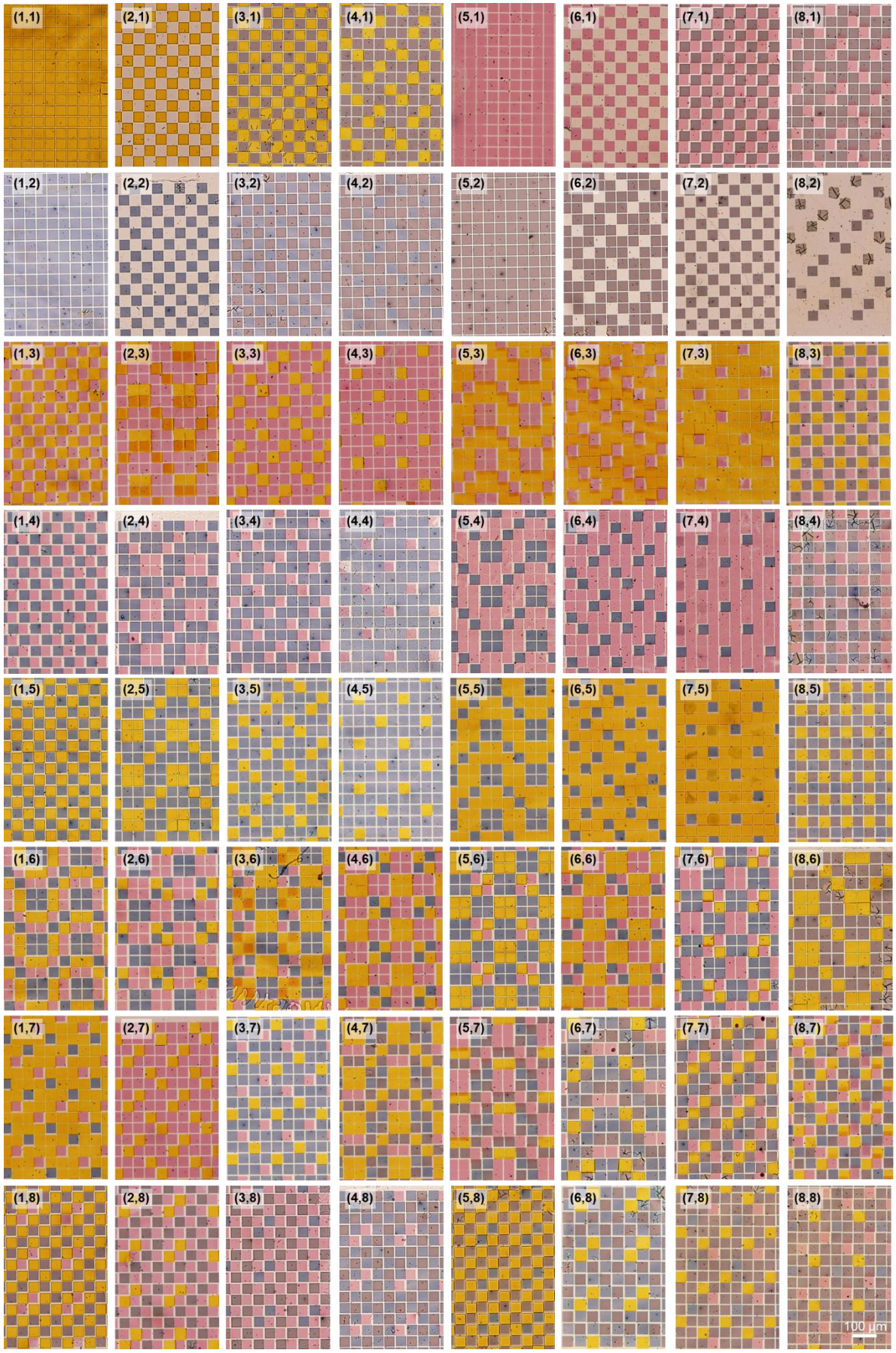

Supplementary Fig. 45. Optical microscopic images of see-through all-polymer full-color electrochromic display.

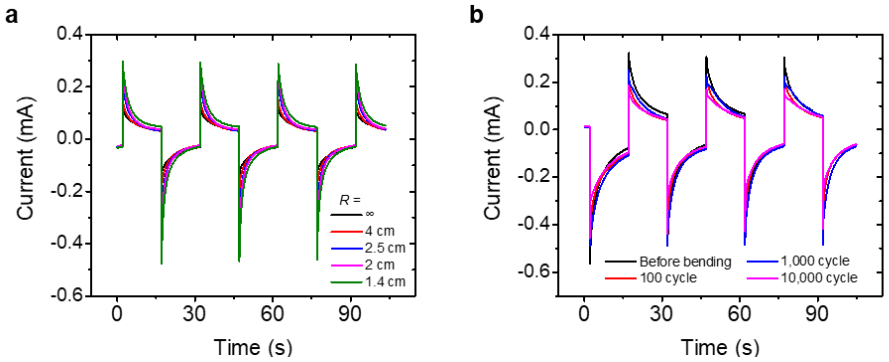

Supplementary Fig. 46. **a**, Transient current of all-polymer electrochromic display in different bending radius. **b**, Transient current of all-polymer electrochromic display in different bending cycle.

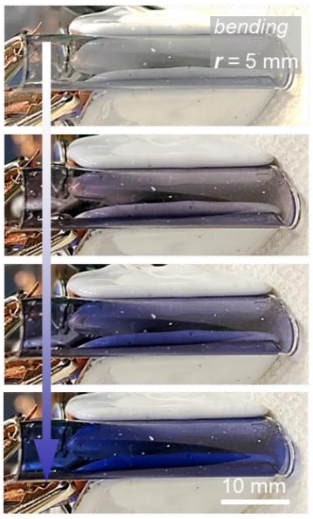

Supplementary Fig. 47. Photographic images of flexible demonstration of all-polymer electrochromic display in bending radius of 0.5 cm.

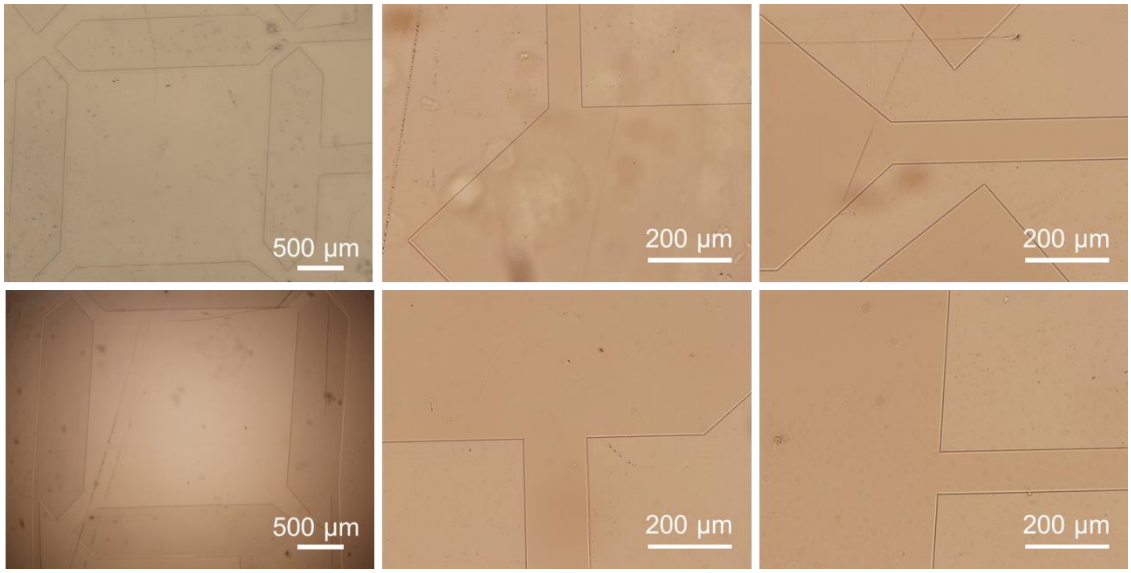

Supplementary Fig. 48. Optical microscopic images of PBDF conductor circuits deposited on PET substrate.

Supplementary Fig. 49. Photographic images of operation of all-polymer segmented electrochromic display in bended condition.

Supplementary Fig. 50. Photographic images of operation of all-polymer segmented electrochromic display on human finger (bending radius = 1.5 cm).

Supplementary Table 1. Thickness, sheet resistance, conductivity, and transmittance of various capacitive transparent conductors for electrochromic devices.

Material	Thickness (nm)	Sheet resistance (Ω sq^{-1})	Conductivity (S cm^{-1})	Transmittance (@550 nm; %)
n-PBDF	7.9[a] (±1.2)[b]	1470[a] (±135)[b]	860[a] (±87)[b]	94.3
	19 (±1.1)	330 (±60)	1700 (±310)	90.3
	25 (±0.9)	250 (±36)	1610 (±340)	88.4
	30 (±1.5)	190 (±23)	1800 (±250)	86.8
	35 (±3.8)	150 (±19)	1940 (±390)	84.1
	39 (±0.9)	130 (±12)	1990 (±200)	80.6
	53 (±2.3)	92 (±14)	2130 (±520)	77.2
	71 (±6.1)	72 (±6)	1980 (±180)	68.5
PEDOT:PSS	33 (±2.2)	314000 (±23100)	0.97 (±0.080)	95.6
	48 (±4.0)	162000 (±14200)	1.30 (±0.11)	93.2
	70 (±3.2)	92000 (±16000)	1.60 (±0.28)	91.8
ITO (8 Ω spec.)	180	8.0 (±0.014)	6930 (±12.2)	90.2
ITO (100 Ω spec.)	30	103 (±2.6)	3240 (±80.9)	98.3
ITO nanoparticles	1730 (±50)	51700 (±4300)	0.11 (±0.009)	92.1
	2030 (±210)	39700 (±3400)	0.12 (±0.013)	88.7

[a]The average values obtained for at least nine points from more than two different batches.
[b]The standard deviation values obtained for at least nine points from more than two different batches.

Supplementary Table 2. Oxidation potential, energy level of HOMO and LUMO, and optical bandgaps of five ECPs.

Material	E_{ox}(V vs. Ag/AgCl)[a]	E_{HOMO}(eV)[a]	E_{LUMO} (eV)[b]	E_g (eV)[b]
Blue	–0.13	–4.28	–2.56	1.72
Cyan	0.39	–4.80	–3.23	1.57
Magenta	0.31	–4.72	–2.72	2.00
Yellow	0.89	–5.20	–2.94	2.26
Black	0.34	–4.76	–3.24	1.52

[a]E_{ox} and E_{HOMO} was calculated in CV curve shown in **Fig. 1f** and **Supplementary Fig. 6**, following equation, $E_{HOMO} = -4.8\ eV - [E_{ox} - E_{1/2Ferrocene}]$.
[b]E_g was estimated to optical bandgap using onset of absorption spectra in neutral state ECPs. E_{LUMO} was calculated from the E_{HOMO} and E_g.

Supplementary Video 1. Recorded video of passive-matrix electrochromic display with 8 × 8 matrix. First, all pixels were fully bleached with positive voltage (+ 1.0 V). A negative voltage (– 0.8 V) was applied to turn on (colored) target pixels line by line along a counter electrode line. After displaying the final graphics, all pixels were bleached again. Delayed time for circuit control was only accelerated. Two videos were integrated in this supplementary video; One is for displaying letter graphics “P”, the other is for “U”.

Supplementary Video 2. Recorded video of all-polymer full-color electrochromic display with 64 colors represented 40 μm size subpixels in lateral arrangement. The colors were tuned by modulating of density of subpixels of four CMYK ECP subpixels. All pixels were fully bleached with positive voltage (+ 1.0 V) and a negative voltage (– 1.0 V) was applied to make pixels colored.

Supplementary Video 3. Recorded video of segmented all-polymer electrochromic display with two 7-segment display for all number representation. Electrochromic graphics were digitally driven using a customed multiplexing multichannel controller with power supply. Fifteen PBDF contact lines and common cathode were applied with positive voltage (+ 1.0 V) and a negative voltage (– 1.0 V) for device bleaching and coloration, respectively. Two videos were integrated in this supplementary video; One is for standard segmented display operation, the other is for segmented display operation on human finger with bending radius of 1.5 cm.

References

S1. Aziz, S.B., Abdullah, O.G., Hussein, A.M. & Ahmed, H.M. From Insulating PMMA Polymer to Conjugated Double Bond Behavior: Green Chemistry as a Novel Approach to Fabricate Small Band Gap Polymers *Polym.* **9**, 626 (2017).

S2. Ke, Z. *et al.* Highly conductive and solution-processable n-doped transparent organic conductor. *J. Am. Chem. Soc.* **145**, 3706-3715 (2023).

S3. Berggren, M. & Malliaras, G.G. How conducting polymer electrodes operate. *Science* **364**, 233-234 (2019).

S4. Li, X. *et al.* Stabilizing hybrid electrochromic devices through pairing electrochromic polymers with minimally color-changing ion-storage materials having closely matched electroactive voltage windows. *ACS Appl. Mater. Interfaces* **13**, 5312-5318 (2021).

S5. Li, X., Wang, X., You, L., Zhao, K. & Mei, J. Improving electrochemical cycling stability of conjugated yellow-to-transmissive electrochromic polymers by regulating effective overpotentials. *ACS Materials Letters* **4**, 336-342 (2022).

S6. Png, R.-Q. *et al.* High-performance polymer semiconducting heterostructure devices by nitrene-mediated photocrosslinking of alkyl side chains. *Nat. Mater.* **9**, 152-158 (2010).

S7. Chen, K. *et al.* Printing dynamic color palettes and layered textures through modeling-guided stacking of electrochromic polymers. *Mater. Horiz.* **9**, 425-432 (2022).

S8. Zhong, Y., Nguyen, G.T.M., Plesse, C., Vidal, F. & Jager, E.W.H. Highly conductive, photolithographically patternable ionogels for flexible and stretchable electrochemical devices. *ACS Appl. Mater. Interfaces* **10**, 21601-21611 (2018).

S9. Pritchard, C.D. *et al.* An injectable thiol-acrylate poly(ethylene glycol) hydrogel for sustained release of methylprednisolone sodium succinate. *Biomaterials* **32**, 587-597 (2011).